Physics Letters B 771 (2017) 13–20

Contents lists available at ScienceDirect

Physics Letters B

www.elsevier.com/locate/physletb

Energy dependence of J/ψ production in Au + Au collisions at $\sqrt{s_{NN}} = 39, 62.4$ and 200 GeV

STAR Collaboration

L. Adamczyk [a], J.K. Adkins [s], G. Agakishiev [q], M.M. Aggarwal [ae], Z. Ahammed [ax], N.N. Ajitanand [an], I. Alekseev [o,z], D.M. Anderson [ap], R. Aoyama [at], A. Aparin [q], D. Arkhipkin [c], E.C. Aschenauer [c], M.U. Ashraf [as], A. Attri [ae], G.S. Averichev [q], X. Bai [g], V. Bairathi [aa], A. Behera [an], R. Bellwied [ar], A. Bhasin [p], A.K. Bhati [ae], P. Bhattarai [aq], J. Bielcik [j], J. Bielcikova [k], L.C. Bland [c], I.G. Bordyuzhin [o], J. Bouchet [r], J.D. Brandenburg [aj], A.V. Brandin [z], D. Brown [w], I. Bunzarov [q], J. Butterworth [aj], H. Caines [bb], M. Calderón de la Barca Sánchez [e], J.M. Campbell [ac], D. Cebra [e], I. Chakaberia [c], P. Chaloupka [j], Z. Chang [ap], N. Chankova-Bunzarova [q], A. Chatterjee [ax], S. Chattopadhyay [ax], X. Chen [ak], J.H. Chen [am], X. Chen [u], J. Cheng [as], M. Cherney [i], W. Christie [c], G. Contin [v], H.J. Crawford [d], S. Das [g], L.C. De Silva [i], R.R. Debbe [c], T.G. Dedovich [q], J. Deng [al], A.A. Derevschikov [ag], L. Didenko [c], C. Dilks [af], X. Dong [v], J.L. Drachenberg [t], J.E. Draper [e], L.E. Dunkelberger [f], J.C. Dunlop [c], L.G. Efimov [q], N. Elsey [az], J. Engelage [d], G. Eppley [aj], R. Esha [f], S. Esumi [at], O. Evdokimov [h], J. Ewigleben [w], O. Eyser [c], R. Fatemi [s], S. Fazio [c], P. Federic [k], P. Federicova [j], J. Fedorisin [q], Z. Feng [g], P. Filip [q], E. Finch [au], Y. Fisyak [c], C.E. Flores [e], J. Fujita [i], L. Fulek [a], C.A. Gagliardi [ap], D. Garand [ah], F. Geurts [aj], A. Gibson [aw], M. Girard [ay], D. Grosnick [aw], D.S. Gunarathne [ao], Y. Guo [r], A. Gupta [p], S. Gupta [p], W. Guryn [c], A.I. Hamad [r], A. Hamed [ap], A. Harlenderova [j], J.W. Harris [bb], L. He [ah], S. Heppelmann [af], S. Heppelmann [e], A. Hirsch [ah], G.W. Hoffmann [aq], S. Horvat [bb], B. Huang [h], H.Z. Huang [f], T. Huang [ab], X. Huang [as], T.J. Humanic [ac], P. Huo [an], G. Igo [f], W.W. Jacobs [n], A. Jentsch [aq], J. Jia [c,an], K. Jiang [ak], S. Jowzaee [az], E.G. Judd [d], S. Kabana [r], D. Kalinkin [n], K. Kang [as], K. Kauder [az], H.W. Ke [c], D. Keane [r], A. Kechechyan [q], Z. Khan [h], D.P. Kikoła [ay], I. Kisel [l], A. Kisiel [ay], L. Kochenda [z], M. Kocmanek [k], T. Kollegger [l], L.K. Kosarzewski [ay], A.F. Kraishan [ao], P. Kravtsov [z], K. Krueger [b], N. Kulathunga [ar], L. Kumar [ae], J. Kvapil [j], J.H. Kwasizur [n], R. Lacey [an], J.M. Landgraf [c], K.D. Landry [f], J. Lauret [c], A. Lebedev [c], R. Lednicky [q], J.H. Lee [c], Y. Li [as], X. Li [ak], W. Li [am], C. Li [ak], J. Lidrych [j], T. Lin [n], M.A. Lisa [ac], Y. Liu [ap], H. Liu [n], F. Liu [g], P. Liu [an], T. Ljubicic [c], W.J. Llope [az], M. Lomnitz [v], R.S. Longacre [c], S. Luo [h], X. Luo [g], G.L. Ma [am], L. Ma [am], Y.G. Ma [am], R. Ma [c], N. Magdy [an], R. Majka [bb], D. Mallick [aa], S. Margetis [r], C. Markert [aq], H.S. Matis [v], K. Meehan [e], J.C. Mei [al], Z.W. Miller [h], N.G. Minaev [ag], S. Mioduszewski [ap], D. Mishra [aa], S. Mizuno [v], B. Mohanty [aa], M.M. Mondal [m], D.A. Morozov [ag], M.K. Mustafa [v], Md. Nasim [f], T.K. Nayak [ax], J.M. Nelson [d], M. Nie [am], G. Nigmatkulov [z], T. Niida [az], L.V. Nogach [ag], T. Nonaka [at], S.B. Nurushev [ag], G. Odyniec [v], A. Ogawa [c], K. Oh [ai], V.A. Okorokov [z], D. Olvitt Jr. [ao], B.S. Page [c], R. Pak [c], Y. Pandit [h], Y. Panebratsev [q], B. Pawlik [ad], H. Pei [g], C. Perkins [d], P. Pile [c], J. Pluta [ay], K. Poniatowska [ay], J. Porter [v], M. Posik [ao], N.K. Pruthi [ae], M. Przybycien [a], J. Putschke [az], H. Qiu [ah], A. Quintero [ao], S. Ramachandran [s], R.L. Ray [aq], R. Reed [w], M.J. Rehbein [i], H.G. Ritter [v], J.B. Roberts [aj], O.V. Rogachevskiy [q], J.L. Romero [e], J.D. Roth [i], L. Ruan [c],

http://dx.doi.org/10.1016/j.physletb.2017.04.078

J. Rusnak [k], O. Rusnakova [j], N.R. Sahoo [ap], P.K. Sahu [m], S. Salur [v], J. Sandweiss [bb], M. Saur [k], J. Schambach [aq], A.M. Schmah [v], W.B. Schmidke [c], N. Schmitz [x], B.R. Schweid [an], J. Seger [i], M. Sergeeva [f], P. Seyboth [x], N. Shah [am], E. Shahaliev [q], P.V. Shanmuganathan [w], M. Shao [ak], A. Sharma [p], M.K. Sharma [p], W.Q. Shen [am], S.S. Shi [g], Z. Shi [v], Q.Y. Shou [am], E.P. Sichtermann [v], R. Sikora [a], M. Simko [k], S. Singha [r], M.J. Skoby [n], N. Smirnov [bb], D. Smirnov [c], W. Solyst [n], L. Song [ar], P. Sorensen [c], H.M. Spinka [b], B. Srivastava [ah], T.D.S. Stanislaus [aw], M. Strikhanov [z], B. Stringfellow [ah], T. Sugiura [at], M. Sumbera [k], B. Summa [af], X. Sun [g], Y. Sun [ak], X.M. Sun [g], B. Surrow [ao], D.N. Svirida [o], A.H. Tang [c], Z. Tang [ak], A. Taranenko [z], T. Tarnowsky [y], A. Tawfik [ba], J. Thäder [v], J.H. Thomas [v], A.R. Timmins [ar], D. Tlusty [aj], T. Todoroki [c], M. Tokarev [q], S. Trentalange [f], R.E. Tribble [ap], P. Tribedy [c], S.K. Tripathy [m], B.A. Trzeciak [j], O.D. Tsai [f], T. Ullrich [c], D.G. Underwood [b], I. Upsal [ac], G. Van Buren [c], G. van Nieuwenhuizen [c], A.N. Vasiliev [ag], F. Videbæk [c], S. Vokal [q], S.A. Voloshin [az], A. Vossen [n], G. Wang [f], Y. Wang [g], F. Wang [ah], Y. Wang [as], J.C. Webb [c], G. Webb [c], L. Wen [f], G.D. Westfall [y], H. Wieman [v], S.W. Wissink [n], R. Witt [av], Y. Wu [r], Z.G. Xiao [as], W. Xie [ah], G. Xie [ak], J. Xu [g], N. Xu [v], Q.H. Xu [al], Y.F. Xu [am], Z. Xu [c], Y. Yang [ab], Q. Yang [ak], C. Yang [al], S. Yang [c], Z. Ye [h], Z. Ye [h], L. Yi [bb], K. Yip [c], I.-K. Yoo [ai], N. Yu [g], H. Zbroszczyk [ay], W. Zha [ak,*], Z. Zhang [am], X.P. Zhang [as], J.B. Zhang [g], S. Zhang [ak], J. Zhang [u], Y. Zhang [ak], J. Zhang [v], S. Zhang [am], J. Zhao [ah], C. Zhong [am], L. Zhou [ak], C. Zhou [am], X. Zhu [as], Z. Zhu [al], M. Zyzak [l]

[a] *AGH University of Science and Technology, FPACS, Cracow 30-059, Poland*
[b] *Argonne National Laboratory, Argonne, Illinois 60439*
[c] *Brookhaven National Laboratory, Upton, New York 11973*
[d] *University of California, Berkeley, California 94720*
[e] *University of California, Davis, California 95616*
[f] *University of California, Los Angeles, California 90095*
[g] *Central China Normal University, Wuhan, Hubei 430079*
[h] *University of Illinois at Chicago, Chicago, Illinois 60607*
[i] *Creighton University, Omaha, Nebraska 68178*
[j] *Czech Technical University in Prague, FNSPE, Prague, 115 19, Czech Republic*
[k] *Nuclear Physics Institute AS CR, 250 68 Prague, Czech Republic*
[l] *Frankfurt Institute for Advanced Studies FIAS, Frankfurt 60438, Germany*
[m] *Institute of Physics, Bhubaneswar 751005, India*
[n] *Indiana University, Bloomington, Indiana 47408*
[o] *Alikhanov Institute for Theoretical and Experimental Physics, Moscow 117218, Russia*
[p] *University of Jammu, Jammu 180001, India*
[q] *Joint Institute for Nuclear Research, Dubna, 141 980, Russia*
[r] *Kent State University, Kent, Ohio 44242*
[s] *University of Kentucky, Lexington, Kentucky, 40506-0055*
[t] *Lamar University, Physics Department, Beaumont, Texas 77710*
[u] *Institute of Modern Physics, Chinese Academy of Sciences, Lanzhou, Gansu 730000*
[v] *Lawrence Berkeley National Laboratory, Berkeley, California 94720*
[w] *Lehigh University, Bethlehem, Pennsylvania 18015*
[x] *Max-Planck-Institut fur Physik, Munich 80805, Germany*
[y] *Michigan State University, East Lansing, Michiagan 48824*
[z] *National Research Nuclear University MEPhI, Moscow 115409, Russia*
[aa] *National Institute of Science Education and Research, Bhubaneswar 751005, India*
[ab] *National Cheng Kung University, Tainan 70101*
[ac] *Ohio State University, Columbus, Ohio 43210*
[ad] *Institute of Nuclear Physics PAN, Cracow 31-342, Poland*
[ae] *Panjab University, Chandigarh 160014, India*
[af] *Pennsylvania State University, University Park, Pennsylyania 16802*
[ag] *Institute of High Energy Physics, Protvino 142281, Russia*
[ah] *Purdue University, West Lafayette, Indiana 47907*
[ai] *Pusan National University, Pusan 46241, Republic of Korea*
[aj] *Rice University, Houston, Texas 77251*
[ak] *University of Science and Technology of China, Hefei, Anhui 230026*
[al] *Shandong University, Jinan, Shandong 250100*
[am] *Shanghai Institute of Applied Physics, Chinese Academy of Sciences, Shanghai 201800*
[an] *State University Of New York, Stony Brook, New York 11794*
[ao] *Temple University, Philadelphia, Pennsylvania 19122*
[ap] *Texas A&M University, College Station, Texas 77843*
[aq] *University of Texas, Austin, Texas 78712*
[ar] *University of Houston, Houston, Texas 77204*
[as] *Tsinghua University, Beijing 100084*
[at] *University of Tsukuba, Tsukuba, Ibaraki, Japan*
[au] *Southern Connecticut State University, New Haven, Connecticut 06515*
[av] *United States Naval Academy, Annapolis, Maryland 21402*
[aw] *Valparaiso University, Valparaiso, Indiana 46383*

[ax] Variable Energy Cyclotron Centre, Kolkata 700064, India
[ay] Warsaw University of Technology, Warsaw 00-661, Poland
[az] Wayne State University, Detroit, Michigan 48201
[ba] World Laboratory for Cosmology and Particle Physics (WLCAPP), Cairo 11571, Egypt
[bb] Yale University, New Haven, Connecticut 06520

ARTICLE INFO

Article history:
Received 26 July 2016
Received in revised form 11 April 2017
Accepted 20 April 2017
Available online 10 May 2017
Editor: M. Doser

ABSTRACT

The inclusive J/ψ transverse momentum spectra and nuclear modification factors are reported at mid-rapidity ($|y| < 1.0$) in Au + Au collisions at $\sqrt{s_{NN}} = 39$, 62.4 and 200 GeV taken by the STAR experiment. A suppression of J/ψ production, with respect to the production in $p + p$ scaled by the number of binary nucleon–nucleon collisions, is observed in central Au + Au collisions at these three energies. No significant energy dependence of nuclear modification factors is found within uncertainties. The measured nuclear modification factors can be described by model calculations that take into account both suppression of direct J/ψ production due to the color screening effect and J/ψ regeneration from recombination of uncorrelated charm–anticharm quark pairs.

1. Introduction

The Relativistic Heavy Ion Collider (RHIC) was built to investigate strongly interacting matter at high temperature and energy density in the laboratory through high-energy heavy-ion collisions. At extremely high temperatures and baryon densities, a transition from the hadronic phase of matter to a new deconfined partonic phase, the Quark–Gluon Plasma (QGP), is predicted by Quantum Chromodynamics (QCD) [1–8]. It has been proposed that the color potential in quarkonia could be screened by quarks and gluons in the QGP [9]. Quarkonia are bound states of charm–anticharm ($c\bar{c}$) or bottom–antibottom ($b\bar{b}$) quark pairs. As a consequence, quarkonium production cross sections in heavy-ion collisions divided by the corresponding number of binary nucleon–nucleon collisions, N_{coll}, are expected to be suppressed compared to those in $p + p$ collisions if QGP is formed in heavy-ion collisions.

The J/ψ is the most abundantly produced quarkonium state accessible to experiments. Over the past twenty years, J/ψ suppression in hot and dense media has been a topic of growing interest. Various measurements of J/ψ production in heavy ion collisions have been performed in different collision systems and at different energies, and indeed a suppression of J/ψ production has been observed [10–13]. A similar centrality dependent suppression was found at SPS (S + U $\sqrt{s_{NN}} = 19.4$ GeV [14], Pb + Pb $\sqrt{s_{NN}} = 17.2$ GeV [15] and In + In $\sqrt{s_{NN}} = 17.2$ GeV [12]) and at RHIC (Au + Au $\sqrt{s_{NN}} = 200$ GeV [16,17]) for mid-rapidity, even though the temperature and energy density reached in these studies are significantly different [18]. Furthermore, a stronger suppression at forward rapidity ($1.2 < |y| < 2.2$) compared to mid-rapidity ($|y| < 0.35$) was observed at RHIC [16]. These observations indicate that effects other than color screening are important for J/ψ production. Among these effects, J/ψ production from the recombination of $c\bar{c}$ [19,20], together with color screening effect, play important roles in explaining the similar suppressions at SPS and RHIC [21]. With the higher temperature and density at RHIC, the increased contribution due to regeneration from the larger charm quark density could compensate for the enhanced suppression. This could also explain a stronger suppression at forward rapidity at RHIC where the charm quark density is lower compared to mid-rapidity [20–23]. In addition to the color screening and regeneration effects, there are also modifications from cold nuclear matter (CNM) effects, such as nuclear parton distribution function modification [24], energy loss by the colliding nuclei [25], Cronin effect [26], and other final state effects, such as nuclear absorption [27] and dissociation by co-movers [28]. The suppression due to these effects has been systematically studied experimentally via $p + A$ collisions [29–39]. However, the extrapolation from $p + A$ to $A + A$ is still model dependent.

The nuclear modification factor of J/ψ production in Pb + Pb collisions at $\sqrt{s_{NN}} = 2.76$ TeV has been measured at the LHC [40–42]. In comparison with results from RHIC in Au + Au collisions at $\sqrt{s_{NN}} = 200$ GeV, the J/ψ production is significantly less suppressed, which suggests significantly more recombination contribution at LHC energies. The measurement of J/ψ production at forward rapidity ($1.2 < |y| < 2.2$) in Au + Au collisions by the PHENIX experiment at $\sqrt{s_{NN}} = 39$ and 62.4 GeV indicates a similar suppression level as that at $\sqrt{s_{NN}} = 200$ GeV [43]. Measurements of J/ψ invariant yields at different collision energies at RHIC in different centralities at mid-rapidity can shed new light on the interplay of the mechanisms for J/ψ production and medium properties.

In this letter, we further study the collision energy dependence of J/ψ production and test the hypothesis of the two competing mechanisms of color screening and regeneration. We present measurements of the J/ψ production at mid-rapidity ($|y| < 1$) with the STAR experiment in Au + Au collisions at $\sqrt{s_{NN}} = 39$, 62.4 using data collected in year 2010 and at $\sqrt{s_{NN}} = 200$ GeV using the combined data in year 2010 [17] and 2011 and study the nuclear modification factors at these energies.

2. Experiment and analysis

The STAR experiment is a large-acceptance multi-purpose detector which covers full azimuth in the pseudorapidity interval $|\eta| < 1$ [44]. The Vertex Position Detector (VPD) was used to select Au + Au collisions that were within ±15 cm of the center of the STAR detector [45]. The minimum-bias trigger utilized in this analysis required a coincidence between the East and West VPD. In order to avoid the VPD inefficiency in peripheral Au + Au collisions, only data in 0–60% central collisions are accepted. The total numbers of 0–60% central events that are used in this analysis are 182 million, 94 million, and 360 million for 39, 62.4 and 200 GeV, respectively. The J/ψ is reconstructed through its decay into electron–positron pairs, $J/\psi \to e^+e^-$ (branching ratio $\mathrm{Br}(J/\psi \to e^+e^-) = 5.97 \pm 0.03\%$ [46]). The primary detectors used in this analysis are the Time Projection Chamber (TPC)

* Corresponding author.
E-mail address: wangmei@rcf.rhic.bnl.gov (W. Zha).

Table I
Summary of centrality bins, average number of participants $\langle N_{part}\rangle$, number of binary collisions $\langle N_{coll}\rangle$, and nuclear overlap function $\langle T_{AA}\rangle$ from MC Glauber simulation of Au + Au at $\sqrt{s_{NN}} = 39$, 62 and 200 GeV. The errors indicate uncertainties from the MC Glauber calculations.

$\sqrt{s_{NN}}$ (GeV)	Centrality (%)	$\langle N_{part}\rangle$	$\langle N_{coll}\rangle$	$\langle T_{AA}\rangle$ (fm^{-2})
39	0–20	273 ± 6	629 ± 26	187 ± 5
	20–40	137 ± 11	245 ± 26	71 ± 7
	40–60	59 ± 10	79 ± 17	23 ±5
	0–60	156 ± 8	316 ± 22	93 ± 6
62	0–20	276 ± 5	664 ± 25	187 ± 5
	20–40	139 ± 10	258 ± 27	71 ± 7
	40–60	60 ± 10	82 ± 18	23 ± 5
	0–60	157 ± 9	332 ± 23	93 ± 6
200	0–20	280 ± 6	785 ± 29	187 ± 5
	20–40	142 ± 11	300 ± 31	71 ± 7
	40–60	62 ± 10	95 ± 21	23 ± 5
	0–60	161 ± 9	393 ± 27	93 ± 6

[47], the Time-of-Flight (TOF) detector [48], and the Barrel Electromagnetic Calorimeter (BEMC) [49]. The TPC provides tracking and particle identification via the ionization energy loss ($\langle dE/dx\rangle$) of charge particles. The TOF [48] measures the velocity of particles, which greatly improved electron identification at low momentum. This detector, combined with the TPC [47], clearly identifies electrons by rejecting hadrons in the low and intermediate momentum range ($p < 1.5$ GeV/c). The BEMC [49], a lead-scintillator calorimeter, is used to improve the electron identification at high momentum ($p > 1.5$ GeV/c). The electron identification method is similar to Refs. [17,50].

Collision centrality was determined from the uncorrected charged particle multiplicity $dN/d\eta$ within $|\eta| < 0.5$ using a Monte Carlo (MC) Glauber model [51]. The dependence of $dN/d\eta$ on the collision vertex position V_z and the beam luminosity has been included to take acceptance and efficiency changes on the measured $dN/d\eta$ into account. For each collision centrality, an average nuclear overlap function, $\langle T_{AA}\rangle$, average number of participants, $\langle N_{part}\rangle$, and average number of binary collisions, $\langle N_{coll}\rangle$, were related to an observed multiplicity range. Centrality definitions in Au + Au collisions for $\sqrt{s_{NN}} = 39$, 62.4 and 200 GeV are summarized in Table I.

The daughter tracks of the J/ψ candidates are required to have at least 25 out of the 45 possible TPC hits, and a distance of closest approach (DCA) from the primary vertex of less than 3 cm. Low momentum ($p < 1.5$ GeV/c) electron and positron candidates are separated from hadrons by selecting on the inverse velocity, $|1/\beta - 1| < 0.03$, where β is the velocity measured in the TOF normalized by the speed of light. The cut value is determined using a three standard deviation window. At high momentum ($p > 1.5$ GeV/c), a cut on the ratio of momentum to energy deposited in towers from BEMC ($0.3 < pc/E < 1.5$) is used to suppress hadrons. The electron and positron candidates are then identified by their specific energy loss ($\langle dE/dx\rangle$) in the TPC. More than 15 TPC hits are required to calculate $\langle dE/dx\rangle$. The normalized $\langle dE/dx\rangle$ is defined as follows:

$$n\sigma_e = \frac{ln(\langle dE/dx\rangle^m / \langle dE/dx\rangle_e^{th})}{R_{dE/dx}} \quad (1)$$

where $\langle dE/dx\rangle^m$ and $\langle dE/dx\rangle^{th}$ represent measured and theoretical values, respectively, and $R_{dE/dx}$ is the experimental $ln(dE/dx)$ resolution. The $n\sigma_e$ cut for electron identification is $-1.5 < n\sigma_e < 2$. The combination of these cuts enables the identification of electrons and positrons over a wide momentum range [17]. The electron sample purity integrated over the measured momentum region is over 90%. Our measurement of J/ψ covers the rapidity range $|y| < 1$ due to the STAR acceptance and decay kinematics.

The J/ψ signal is extracted by subtracting combinatorial background reconstructed from the unlike-sign mixed-events spectrum. The like-sign distributions can be used as normalization references for the mixed-events method. The like-sign and mixed-events distributions are obtained as follows:

1) Like-sign: Electrons (or positrons) of the same charge sign are paired within the same event.
2) Mixed-events: Events are categorized according to the position along the beam line of the primary vertex and centrality of the event. Electrons from one event are paired with positrons from other random events from an event pool with similar global features such as collision centrality and vertex position. The vertex position is divided into 20 bins and the event centrality into 10 bins to ensure that the mixing is done using tracks from similar conditions.

The invariant mass distribution of e^+e^- pairs before and after the combinatorial background subtraction in 0–60% central Au + Au collisions are shown in Fig. 1 for $\sqrt{s_{NN}} = 39$, 62.4, and 200 GeV. The mixed-event background is normalized to the like-sign distribution in a mass range of 2.0–4.0 GeV/c^2 and the normalized shapes show close agreement. The normalization technique is described in Ref. [52]. The mass distribution of e^+e^- is fitted by the J/ψ signal shape obtained from MC simulation, which includes the resolution of the TPC, bremsstrahlung of the daughter electrons in the detector and internal radiation of J/ψ, combined with a straight line for residual background. The residual background mainly comes from the correlated open charm decays and Drell–Yan processes. The raw J/ψ signal is obtained from bin counting in the mass range 2.7–3.2 GeV/c^2 after combinatorial and residual background subtraction. The fraction of J/ψ counts outside of the mass window was determined from the J/ψ MC simulated signal shape and was found to be ∼9%. This was used to correct the number of J/ψ counts. Signal-to-background ratios for these three energies are observed to be 0.62, 0.39, and 0.04, respectively for the transverse momentum (p_T) interval 0–3 GeV/c (39 and 62 GeV) and 0–5 GeV/c (200 GeV). The J/ψ invariant yield is defined as

$$\mathrm{Br}_{J/\psi\to e^+e^-}\frac{d^2N}{2\pi\, p_T dp_T dy} = \frac{1}{2\pi\, p_T \Delta p_T \Delta y}\frac{N_{J/\psi\to e^+e^-}}{A\epsilon N_{EVT}} \quad (2)$$

where $N_{J/\psi\to e^+e^-}$ is the uncorrected number of reconstructed J/ψ, N_{EVT} is the number of events in the relevant Au + Au centrality selection, $A\epsilon$ is the detector's geometric acceptance times its efficiency (about 0.05 ∼ 0.12 depending on p_T, centrality and collision energy), and Δp_T and Δy are the bin width in p_T and y, respectively. Acceptance and efficiency corrections (TPC and BEMC related) are estimated by MC simulations with GEANT3 package [53]. Some of the efficiency corrections such as those corresponding to the TOF and dE/dx related cuts are extracted directly from data [52]. The acceptance and efficiency correction procedure is similar to Refs. [17,50].

The systematic uncertainties in this analysis include uncertainties from the particle identification efficiency using the TPC, TOF, and BEMC, the tracking efficiency from TPC, and the yield extraction methods. The systematic uncertainty on the efficiency correction and particle identification is estimated by comparing the difference for the related cut distributions between simulation and data. In order to account for the contributions from radiation losses and correlated background in the yield extraction procedure, the mass window and methods for signal counting have also been varied to evaluate the uncertainties. Table II contains a summary of

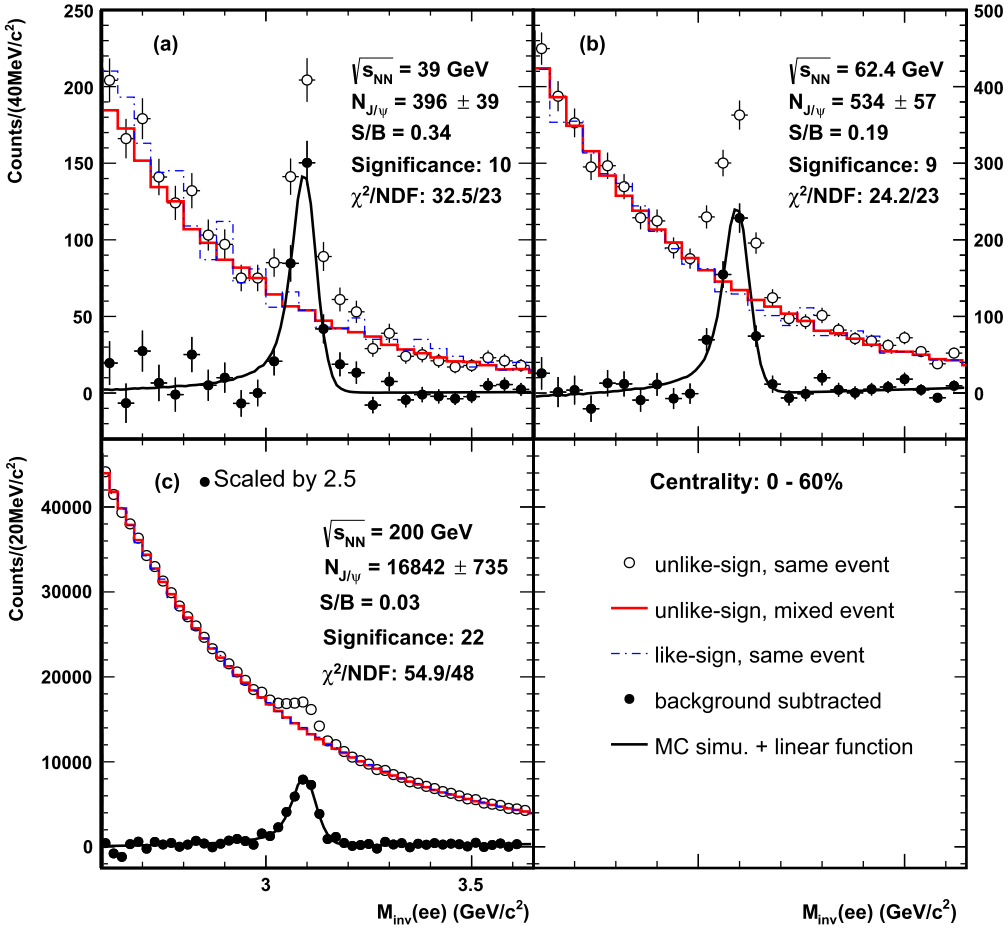

Fig. 1. The e^+e^- invariant mass distribution of J/ψ candidates (black open circles), like-sign combinatorial background (blue dashed line), mixed event combinatorial background (red solid line), and J/ψ candidates with mixed event background subtracted (black solid circles) in Au + Au collisions at $\sqrt{s_{NN}}$ = 39 (a), 62.4 (b), and 200 GeV (c) for centrality 0–60%. The J/ψ signal shape from a MC simulation is combined with a linear residual background and is fitted to the combinatorial background subtracted data (black solid line). (For interpretation of the references to color in this figure legend, the reader is referred to the web version of this article.)

the contributions from the different sources. The ranges in the table are corresponding to the p_T, centrality and collision energy dependence of uncertainties. The uncertainties are partially correlated among the p_T and centrality intervals. The total systematic uncertainties in the integrated p_T range are 20%, 11%, and 10% at $\sqrt{s_{NN}}$ = 39, 62.4, and 200 GeV, respectively. At $\sqrt{s_{NN}}$ = 39 GeV, the large systematic uncertainty on the particle identification BEMC related cuts is due to the large uncertainties associated to the cuts themselves. The normalization uncertainty on the nuclear modification factor includes the uncertainty from $\langle T_{AA}\rangle$ and the statistical and systematic uncertainty of the J/ψ cross section in $p + p$. The centrality and transverse momentum dependence of the total systematic uncertainties are reflected in the results shown in Section 3.

3. Results

The J/ψ invariant yields as a function of p_T in Au + Au collisions at $\sqrt{s_{NN}}$ = 39, 62.4, and 200 GeV for different centrality bins are shown in Fig. 2. As expected, the J/ψ invariant yields are larger in Au + Au collisions at larger center-of-mass energies. Results from the current measurements (year 2011) are compared with the published results from data taken in 2010, they show close agreement with each other. These two measurements are combined together to cumulate more statistics for the nuclear modification factors in this paper.

Table II
The contributions of systematic uncertainty sources for $\sqrt{s_{NN}}$ = 39, 62.4 and 200 GeV. The uncertainties are partially correlated among the p_T and centrality intervals.

Systematic uncertainty source	39 GeV	62.4 GeV	200 GeV
TPC tracking cuts (%)	8	7	6
BEMC related cuts (%)	17–25	3–5	1–2
TOF related cuts (%)	2	2	2
Yield extraction (%)	6–12	2–7	5–11
Total (%)	19–29	10–12	8–12
$\langle N_{coll}\rangle$ (%)	4–22	4–22	4–22
$\langle T_{AA}\rangle$ (%)	3–22	3–22	3–22
$\sigma^{pp}_{J/\psi}$ (%)	12	7	14

Nuclear modification factors (R_{CP}, R_{AA}) are used to quantify the suppression of J/ψ production. R_{CP} is a ratio of the J/ψ yield in central collisions to peripheral collisions (centrality: 40–60%) and defined as follows:

$$R_{CP} = \frac{\frac{dN/dy}{\langle N_{coll}\rangle}(central)}{\frac{dN/dy}{\langle N_{coll}\rangle}(peripheral)} \quad (3)$$

where $\langle N_{coll}\rangle$ and dN/dy are the average number of nucleon–nucleon collisions and J/ψ yield in a given centrality, respectively. dN/dy is obtained from the integration of the J/ψ p_T spectrum. The extrapolation of the p_T spectrum to the full coverage ($p_T > 0$ GeV/c) is based on the two following functions:

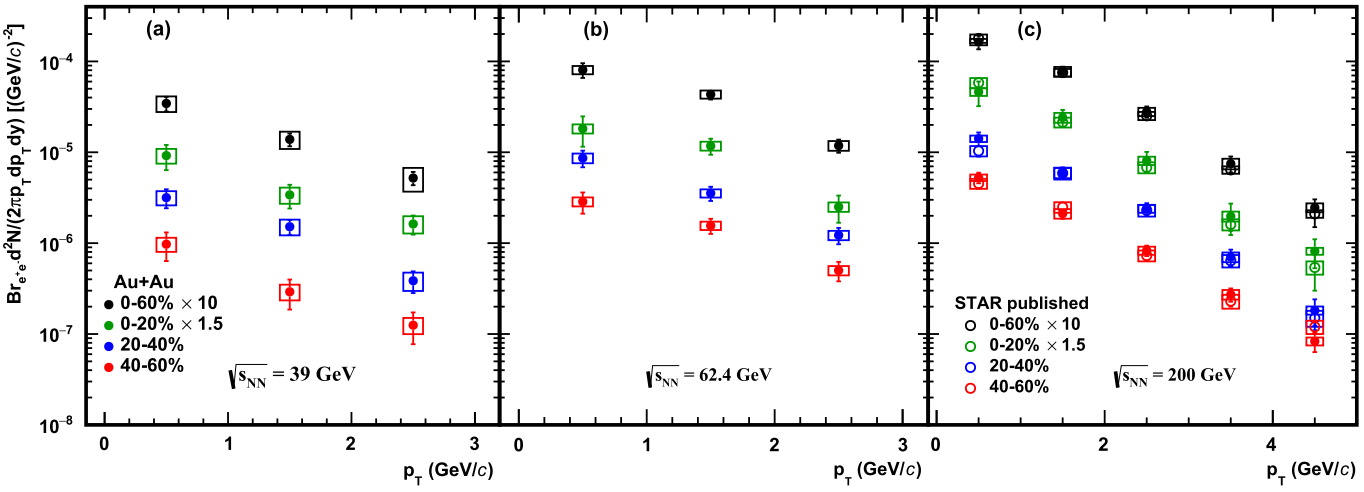

Fig. 2. J/ψ invariant yields in Au + Au collisions at $\sqrt{s_{NN}}$ = 39, 62.4 and 200 GeV as a function of p_T for different centralities. The error bars represent the statistical uncertainties. The boxes represent the systematic uncertainties. The STAR published results are from Refs. [50] and [17].

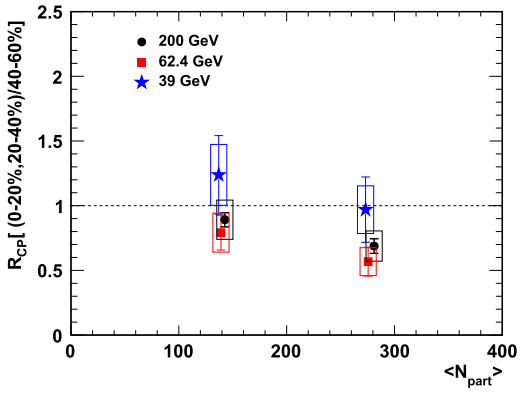

Fig. 3. J/ψ R_{CP} results (with respect to 40–60% peripheral collisions) for Au + Au as a function of $\langle N_{part}\rangle$. The error bars represent the statistical uncertainties. The boxes represent the systematic uncertainties combined with uncertainties from $\langle N_{coll}\rangle$ in different centrality bins.

$$\frac{dN}{dp_T} = a \times \frac{p_T}{(1+b^2p_T^2)^n} \tag{4}$$

$$\frac{dN}{dp_T} = l \times p_T \times \exp^{-\frac{m_T}{h}}, \qquad m_T = \sqrt{p_T^2 + m_{J/\psi}^2} \tag{5}$$

where a, b, n, h and l are free parameters. The fit results from Eq. (4) have been assigned as central value, and the differences ($< 2\%$) between these two functional fits have been taken as a source of systematic uncertainty. Note that R_{CP} reflects only relative suppression – if the modification of J/ψ yield in central and peripheral bins is the same, R_{CP} is equal to 1. The R_{CP}, as a function of the average number of participant nucleons ($\langle N_{part}\rangle$), for Au + Au collisions at $\sqrt{s_{NN}}$ = 39, 62.4 and 200 GeV, are shown in Fig. 3. Note that the peripheral bin selection is 40–60% central Au + Au collisions for these three energies. The systematic uncertainties for R_{CP} are mainly from $\langle N_{coll}\rangle$ and yield extraction. Systematic uncertainties originating from TPC, BEMC and TOF related cuts, are negligible or mostly cancel. A suppression is observed in central Au + Au collisions at $\sqrt{s_{NN}}$ = 62.4 GeV, which is similar to that at $\sqrt{s_{NN}}$ = 200 GeV.

R_{AA} is obtained from comparing J/ψ production in A + A collisions to $p + p$ collisions, defined as follows:

$$R_{AA} = \frac{1}{\langle T_{AA}\rangle} \frac{d^2N_{AA}/dp_T dy}{d^2\sigma_{pp}/dp_T dy} \tag{6}$$

where $d^2N_{AA}/dp_T dy$ is the J/ψ yield in A + A collisions and $d^2\sigma_{pp}/dp_T dy$ is the J/ψ cross section in $p + p$ collisions. The nuclear overlap function with impact parameter **b** is defined as $T_{AA}(\mathbf{b}) = \int T_A(\mathbf{s})T_A(\mathbf{s}-\mathbf{b})d^2s$, where $T_A(\mathbf{s})$ is the probability per unit transverse area of a nucleon being located in the target flux tube. The uncertainties from T_{AA} are estimated by varying the radius and skin depth of the nuclei in the Glauber calculations. If there are no hot or cold nuclear matter effects, the value of R_{AA} should be unity.

To obtain R_{AA} at $\sqrt{s_{NN}}$ = 39 and 62.4 GeV, we have to derive the J/ψ cross section in $p + p$ collisions because there are no measurements available for the $p + p$ references at STAR for these two energies. There are several $p + p$ measurements from fixed target p + A experiments [54–56] and from Intersecting Storage Ring (ISR) collider experiments [57,58] near these two energies. However, the p_T shapes from Ref. [57] and Ref. [58] at $\sqrt{s}$ = 63 GeV are inconsistent with each other and the cross section measurements at $\sqrt{s}$ = 39 GeV are comparable to (or even larger than) that at $\sqrt{s}$ = 63 GeV. Therefore, we use the cross section derived in Ref. [59] as our $p + p$ reference baselines for $\sqrt{s_{NN}}$ = 39 and 62.4 GeV. In Ref. [59], the world-wide experimental data on J/ψ cross sections and kinematic distributions in $p + p$ and p + A collisions at $\sqrt{s}$ = 6.8–7000 GeV are examined in a systematic way. The authors explore the $\sqrt{s}$ dependence of the inclusive cross section, rapidity and transverse momentum distributions phenomenologically and develop a strategy for the interpolation of the J/ψ cross section and kinematics at RHIC energies. This approach is found to describe the world-wide J/ψ data reasonably well. With this strategy, the predicted J/ψ cross section times branching ratio at $\sqrt{s}$ = 39 and 62.4 GeV in mid-rapidity are $\mathrm{Br}(J/\psi \to e^+e^-)d\sigma/dy|_{|y|<1.0} = 9.0 \pm 0.6$ and 17.6 ± 2.1 nb, respectively.

With the derived $p + p$ references for $\sqrt{s}$ = 39 and 62.4 GeV, and the measured $p + p$ baseline at $\sqrt{s}$ = 200 GeV [50,60], we obtain the R_{AA} of J/ψ for $p_T > 0$ as a function of $\langle N_{part}\rangle$ in Au + Au collisions at $\sqrt{s_{NN}}$ = 39, 62.4, and 200 GeV, as shown in Fig. 4 (a). The p_T-differential J/ψ R_{AA} is shown in Fig. 4 (b). The bars and boxes on the data points represent the statistical and systematic uncertainties, respectively. The shaded and hatched bands indicate the uncertainties on the baseline J/ψ cross section in $p + p$ collisions [50,59,60] and $\langle T_{AA}\rangle$, respectively. The bands on the vertical axes indicate global uncertainties, while those on the data points represent bin to bin uncertainties. The measurements from SPS [12,14,15] and LHC [61] and the expected R_{AA} with complete

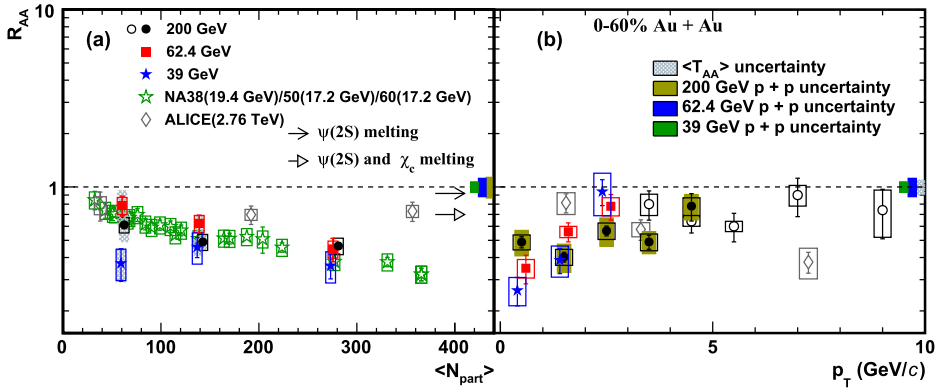

Fig. 4. The results of J/ψ R_{AA} as a function of $\langle N_{part}\rangle$ (a) and p_T (b) in Au + Au collisions at $\sqrt{s_{NN}}$ = 39, 62.4 and 200 GeV. The error bars represent the statistical uncertainties. The boxes represent the systematic uncertainties. The shaded and hatched bands indicate the uncertainties on the baseline J/ψ cross section in $p+p$ collisions [50,59,60] and $\langle T_{AA}\rangle$, respectively. The ALICE points are from [61]. The ratio of feed-down J/ψ from higher chamonium states to inclusive J/ψ is from [63]. The STAR high-p_T ($3 < p_T < 10$ GeV/c) results, represented as open circles, are from [50].

$\psi(2S)$ and χ_c melting and no modification of the J/ψ yield [63] are also included for comparison. Suppression of J/ψ production is observed in Au + Au collisions from $\sqrt{s_{NN}}$ = 39 to 200 GeV with respect to the production in $p+p$ scaled by $\langle T_{AA}\rangle$. For R_{AA} as a function of $\langle N_{part}\rangle$, no significant energy dependence is observed within uncertainties from $\sqrt{s_{NN}}$ = 17.2 to 200 GeV. For the J/ψ R_{AA} as a function of p_T, significant suppression is observed at low p_T ($p_T < 2$ GeV/c) from $\sqrt{s_{NN}}$ = 39 to 200 GeV. The modification of J/ψ production is consistent within the systematic uncertainties for these collision energies. The ALICE [61] points are also shown for comparison. As shown in the figure, the ALICE R_{AA} results are higher than the measurements at RHIC and SPS and show a different trend as a function of p_T. Fig. 5 shows the comparison of R_{AA} between mid-rapidity from STAR and forward rapidity from PHENIX from $\sqrt{s_{NN}}$ = 39 to 200 GeV. The suppression of J/ψ shows no significant rapidity dependence at $\sqrt{s_{NN}}$ = 39 nor 62.4 GeV within uncertainties.

As shown in Fig. 6, theoretical calculations [21] with initial suppression and J/ψ regeneration describe the data within 1.6 standard deviation for these three collision energies. The R_{AA} results as a function of collision energy for 0–20% centrality are also shown in Fig. 7. Theoretical calculations are also included for comparison. The calculations include two components: direct suppression and

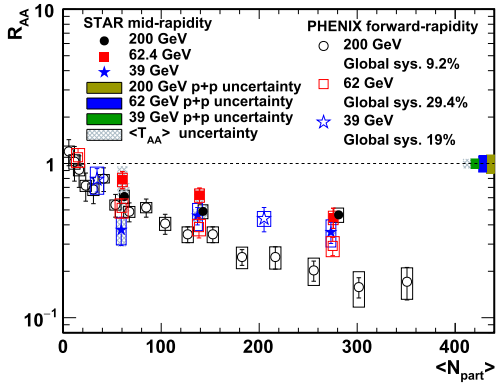

Fig. 5. J/ψ R_{AA} results as a function of $\langle N_{part}\rangle$ in Au + Au collisions at $\sqrt{s_{NN}}$ = 39, 62.4 and 200 GeV. The error bars represent the statistical uncertainties. The boxes represent the systematic uncertainties. The shaded and hatched bands indicate the uncertainties on the baseline J/ψ cross section in $p+p$ collisions [50,59,60] and $\langle T_{AA}\rangle$, respectively. The PHENIX results are from [43,62].

regeneration. The direct suppression represent the "anomalous" suppression of primordial J/ψs due to CNM and color screening effects. According to the model calculations [21], the R_{AA} is about

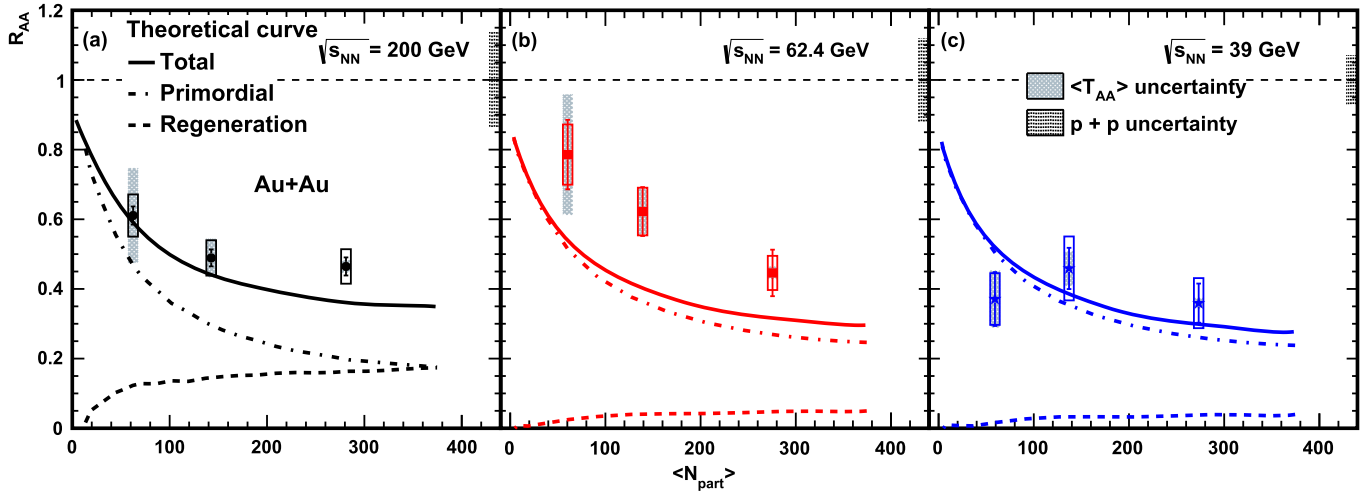

Fig. 6. The results of J/ψ R_{AA} as a function of $\langle N_{part}\rangle$, in comparison with model calculations [21], for Au + Au collisions at $\sqrt{s_{NN}}$ = 200 (a), 62.4 (b) and 39 GeV (c), respectively. The error bars represent the statistical uncertainties. The boxes represent the systematic uncertainties. The dotted and hatched bands indicate the uncertainties on the baseline J/ψ cross section in $p+p$ collisions [50,59,60] and $\langle T_{AA}\rangle$, respectively. Solid lines are J/ψ modification factors from model [21]; dash-dotted line are suppressed primordial production; dashed lines are regeneration component.

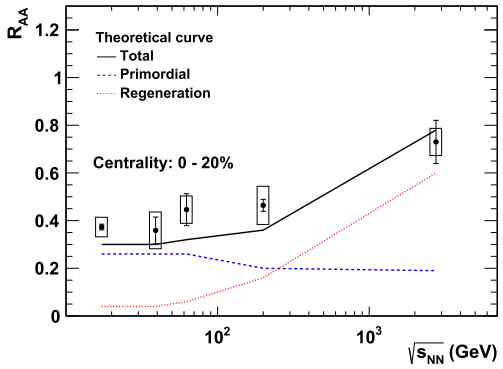

Fig. 7. The results of J/ψ R_{AA} as a function of collision energy for centrality 0–20%, in comparison with model calculations [21]. The SPS result ($\sqrt{s_{NN}} = 17.2$ GeV) is from [10,15]; the ALICE point ($\sqrt{s_{NN}} = 2.76$ TeV) is from [61]. The error bars represent the statistical uncertainties and the boxes represent the systematic uncertainties. The boxes include the systematic uncertainties, the uncertainties on the baseline J/ψ cross section in $p+p$ collisions [50,59,60] and the uncertainties from $\langle T_{AA}\rangle$. Solid line is the total J/ψ modification factors from model; dash-dotted line is the suppressed primordial production; dashed line is the regeneration component. The theory calculations are only done for the five specific energy points, and connected by straight lines. Note: since ALICE data show no significant centrality dependence, it is appropriate to use the available 0–10% data at 2.76 TeV in this figure.

0.6 for central Au + Au collisions at $\sqrt{s_{NN}} = 200$ GeV with only CNM effects. The regeneration component is responsible for the contribution from the recombination of correlated or uncorrelated $c\bar{c}$ pairs. The feed-down to J/ψ from χ_c and ψ' has been taken into account in the calculations. No significant energy dependence of R_{AA} for 0–20% centrality is observed at $\sqrt{s_{NN}} < 200$ GeV. As the collision energy increases the QGP temperature increases, thus the J/ψ color screening becomes more significant. However, in the theoretical calculation [21], the regeneration contribution increases with collision energy due to the increase in the charm pair production, and compensates the enhanced suppression arising from the higher temperature. The higher R_{AA} at ALICE may indicate that the surviving J/ψs are mainly coming from the recombination contribution. The model calculation describes the energy dependence of J/ψ production from SPS to LHC.

4. Summary

In summary, we report on recent STAR measurements of J/ψ production at mid-rapidity in Au + Au collisions at $\sqrt{s_{NN}} = 39$, 62.4 and 200 GeV. Suppression of J/ψ production, with respect to the production in $p+p$ scaled by the number of binary nucleon–nucleon collisions, is observed at these three energies. No significant energy dependence of the nuclear modification factor (either R_{AA} or R_{CP}) is found within uncertainties. Model calculations, which include direct suppression and regeneration, reasonably describe the centrality and energy dependence of J/ψ production in high-energy heavy ion collisions.

Acknowledgements

We thank the RHIC Operations Group and RCF at BNL, the NERSC Center at LBNL, the KISTI Center in Korea, and the Open Science Grid consortium for providing resources and support. This work was supported in part by the Office of Nuclear Physics within the U.S. DOE Office of Science, the U.S. NSF, the Ministry of Education and Science of the Russian Federation, NSFC, CAS, MoST and MoE of China, the National Research Foundation of Korea, NCKU (Taiwan), GA and MSMT of the Czech Republic, FIAS of Germany, DAE, DST, and UGC of India, the National Science Centre of Poland, National Research Foundation, the Ministry of Science, Education and Sports of the Republic of Croatia, and RosAtom of Russia.

References

[1] E.V. Shuryak, Phys. Rep. 61 (1980) 71.
[2] S. Digal, P. Petreczky, H. Satz, Phys. Rev. D 64 (2001) 094015.
[3] F. Karsch, D. Kharzeev, H. Satz, Phys. Lett. B 637 (2006) 75.
[4] P. Braun-Munzinger, J. Stachel, Nature 448 (2007) 302.
[5] J. Adams, et al., STAR Collaboration, Nucl. Phys. A 757 (2005) 102.
[6] K. Adcox, et al., PHENIX Collaboration, Nucl. Phys. A 757 (2005) 184.
[7] B.B. Back, et al., PHOBOS Collaboration, Nucl. Phys. A 757 (2005) 28.
[8] I. Arsene, et al., BRAHMS Collaboration, Nucl. Phys. A 757 (2005) 1.
[9] T. Matsui, H. Satz, Phys. Lett. B 178 (1986) 416.
[10] L. Kluberg, Eur. Phys. J. C 43 (2005) 145.
[11] M.C. Abreu, et al., Phys. Lett. B 449 (1999) 128.
[12] R. Arnaldi, et al., Phys. Rev. Lett. 99 (2007) 132302.
[13] E.T. Atomssa, Eur. Phys. J. C 61 (2009) 683.
[14] M.C. Abreu, et al., Phys. Lett. B 466 (1999) 408.
[15] M.C. Abreu, et al., Phys. Lett. B 477 (2000) 28.
[16] A. Adare, et al., Phys. Rev. Lett. 98 (2007) 232301.
[17] L. Adamczyk, et al., Phys. Rev. C 90 (2014) 024906.
[18] K.J. Eskola, et al., Nucl. Phys. B 570 (2000) 379.
[19] P. Braun-Munzinger, J. Stachel, Phys. Lett. B 490 (2000) 196.
[20] L. Grandchamp, R. Rapp, G.E. Brown, Phys. Rev. Lett. 92 (2004) 212301.
[21] X. Zhao, R. Rapp, Phys. Rev. C 82 (2010) 064905 (private communication).
[22] R. Rapp, et al., Prog. Part. Nucl. Phys. 65 (2010) 209.
[23] Y. Liu, et al., Int. J. Mod. Phys. E 24 (2015) 1530015.
[24] J.L. Nagle, et al., Phys. Rev. C 84 (2011) 044911.
[25] J.L. Nagle, M.J. Bennett, Phys. Lett. B 465 (1999) 21.
[26] J.W. Cronin, et al., Phys. Rev. D 11 (1975) 3105.
[27] R. Vogt, Nucl. Phys. A 700 (2002) 539.
[28] E.G. Ferreiro, Phys. Lett. B 749 (2015) 98.
[29] D. Alde, et al., Phys. Rev. Lett. 66 (1991) 133.
[30] M. Leitch, et al., Nucl. Phys. A 544 (1992) 197c.
[31] M. Leitch, et al., Phys. Rev. Lett. 84 (2000) 3256.
[32] B. Alessandro, et al., Eur. Phys. J. C 33 (2004) 31.
[33] B. Alessandro, et al., Eur. Phys. J. C 39 (2005) 335.
[34] R. Arnaldi, et al., Phys. Lett. B 706 (2012) 263.
[35] A. Adare, et al., Phys. Rev. C 87 (2013) 034904.
[36] A. Adare, et al., Phys. Rev. Lett. 107 (2011) 142301.
[37] A. Adare, et al., Phys. Rev. Lett. 111 (2013) 202301.
[38] B. Abelev, et al., J. High Energy Phys. 02 (2014) 073.
[39] W.K. Brooks (for ATLAS Collaboration), Nucl. Part. Phys. Proc. 276–278 (2016) 149.
[40] B. Abelev, et al., Phys. Rev. Lett. 109 (2012) 072301.
[41] G. Aad, et al., Phys. Lett. B 697 (2011) 294.
[42] S. Chatrchyan, et al., J. High Energy Phys. 05 (2012) 063.
[43] A. Adare, et al., Phys. Rev. C 86 (2012) 064901.
[44] K.H. Ackermannn, et al., Nucl. Instrum. Methods A 499 (2003) 624.
[45] W.J. Llope, et al., Nucl. Instrum. Methods 759 (2014) 23.
[46] K.A. Olive, et al., Chin. Phys. C 38 (2014) 090001.
[47] M. Anderson, et al., Nucl. Instrum. Methods 499 (2003) 659.
[48] W.J. Llope, Nucl. Instrum. Methods 661 (2012) S110.
[49] M. Beddo, et al., Nucl. Instrum. Methods 499 (2003) 725.
[50] L. Adamczyk, et al., Phys. Lett. B 722 (2013) 55.
[51] M.L. Miller, et al., Annu. Rev. Nucl. Part. Sci. 57 (2007) 205.
[52] L. Adamczyk, et al., Phys. Rev. C 92 (2015) 024912.
[53] B.I. Abelev, et al., Phys. Rev. C 79 (2009) 034909.
[54] T. Alexopoulos, et al., Phys. Rev. D 55 (1997) 3927.
[55] M.H. Schub, et al., Phys. Rev. D 52 (1995) 1307.
[56] A. Gribushin, et al., Phys. Rev. D 62 (2000) 012001.
[57] A.G. Clark, et al., Nucl. Phys. B 142 (1978) 29.
[58] C. Kourkoumelis, et al., Phys. Lett. B 91 (1980) 481.
[59] W. Zha, et al., Phys. Rev. C 93 (2016) 024919.
[60] A. Adare, et al., Phys. Rev. D 82 (2010) 012001.
[61] B. Abelev, et al., Phys. Lett. B 734 (2014) 314.
[62] A. Adare, et al., Phys. Rev. C 84 (2011) 054912.
[63] P. Faccioli, et al., J. High Energy Phys. 10 (2008) 004.